ORIGINAL ARTICLE

lajss.org
Latin American Journal of Solids and Structures

www.lajss.org

Optimal Design of Non-linear Truss Structures considering Progressive Collapse

Túlio Raunyr Cândido Felipe[a*], André Teófilo Beck[b]

[a]Marinha do Brasil – MB, Diretoria de Obras Civis da Marinha, Rio de Janeiro, RJ, Brasil. E-mail: tulio.raunyr@gmail.com
[b]Universidade de São Paulo – USP, Escola de Engenharia de São Carlos, Departamento de Engenharia de Estruturas, São Carlos, SP, Brasil. E-mail: atbeck@sc.usp.br

*Corresponding author

https://doi.org/10.1590/1679-78257812

Abstract

In this paper, a methodology is proposed to evaluate the optimal design of truss structures considering progressive collapse. This methodology combines Total-Lagrangian formulation for material and geometrical nonlinear analysis, using nodal positions and log-strain measure; the Systematic Reliability-based Approach to Progressive Collapse method; and risk-optimization formulation. Two benchmark examples are analyzed and discussed. The results demonstrate the accuracy, robustness, and efficiency of the proposed methodology in evaluation the optimal design of truss structures subjected to progressive collapse. It is shown that material behavior (elastic, elastoplastic, and hyperelastic) and rate of loading (step and linear load) can lead to different optimal design configurations. In the redundant hyperstatic truss example, the coefficient of vulnerability identifies the most critical bar for each truss configuration. The most vulnerable bars in the reference design become less vulnerable in the optimal design, leading to load redistribution, or alternate load paths, which reduce the probability of occurrence of progressive collapse.

Keywords

progressive collapse; truss structures; non-linear behavior; optimal design.

Graphical abstract

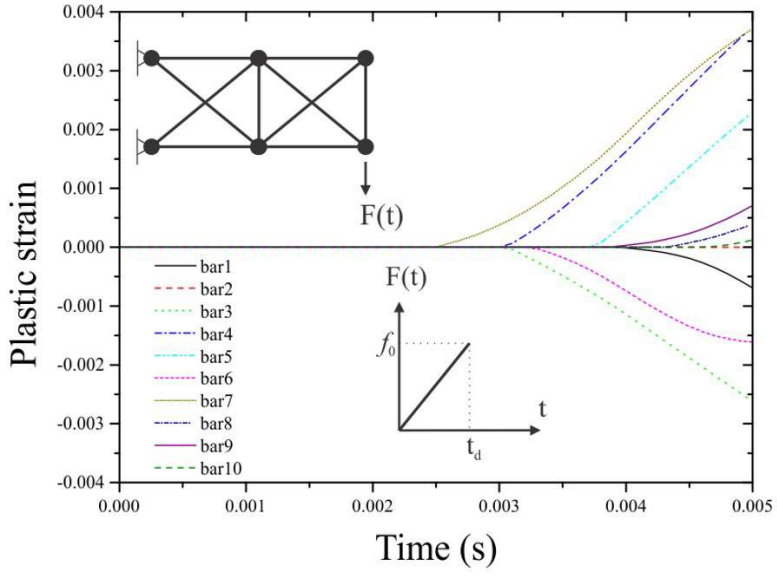

Received: August 23, 2023. In revised form: May 13, 2024. Accepted: May 25, 2024. Available online: June 10, 2024
https://doi.org/10.1590/1679-78257812

Latin American Journal of Solids and Structures. ISSN 1679-7825. Copyright © 2024. This is an Open Access article distributed under the terms of the Creative Commons Attribution License, which permits unrestricted use, distribution, and reproduction in any medium, provided the original work is properly cited.

1 INTRODUCTION

Truss structures, composed of interconnected elements forming triangular units, are ubiquitous in engineering and construction. From bridges to transmission towers and offshore platforms, truss elements are favored due to their low cost and high mechanical efficiency. However, despite their widespread use, uncertainties inherent in the structural response pose significant challenges in assessing their mechanical behavior, especially concerning progressive collapse events.

A mechanical model of truss structures, grounded in solid mechanics principles, assumes known material properties, actions, and boundary conditions. These assumptions, while facilitating analysis, ignore uncertainties that must be accounted for to ensure a robust assessment of structural behavior (Felipe and Beck 2021). Progressive collapse events, triggered by abnormal loads characterized by low occurrence probabilities, high intensities, randomness, and extreme consequences, further emphasize the need to consider uncertainties.

In engineering problems, uncertainties can be classified as intrinsic and epistemic (Melchers and Beck 2018). Intrinsic uncertainties, quantifiable in terms of probabilities, are adequately addressed through structural reliability analysis, which calculates the probability of failure. Epistemic uncertainties, on the other hand, include non-structural factors like unpredictable loads, manufacturing quality, workmanship, and human errors (Beck 2020, Beck et al. 2023), which can be addressed through comprehensive risk analysis (Ayyub and Klir 2006).

While research on optimal structural design considering uncertainties has been extensive, there remains a gap concerning the optimization of truss structures against progressive collapse. Existing studies employ methods like Reliability-Based Design Optimization and Risk Optimization, yet few consider the specific challenges posed by truss structures and the implications of progressive collapse (Gomes and Beck 2014; Liu et al. 2016; Saad et al. 2018; Tessari et al. 2019; Zaman and Mahadevan 2017), (Rodrigues da Silva et al. 2024).

Addressing this gap, this paper focuses on optimizing truss structures parametrically while considering uncertainties and the potential for progressive collapse. It emphasizes the necessity of accurate modeling of component failure and system collapse, incorporating comprehensive material failure models and dynamic finite element analysis accounting for material and geometrical nonlinearities.

The study compares the effects of geometrical and material nonlinearities on the optimal design of truss structures, exploring fragile and ductile material models and the discrepancies between static and dynamic analyses. Results demonstrate the significant influence of analysis type and truss material on the optimal cross-section areas of bar elements, providing insights for engineers and designers seeking to enhance the structural performance and resilience of truss systems against progressive collapse.

2 MECHANICAL MODELLING

In this paper, a Total-Lagrangian formulation for material and geometrical nonlinear analysis is employed in the mechanical analysis of truss structures. The model employs a log-strain measure (ε), which is decomposed in elastic and plastic terms. The model assumes: decoupling between elasticity-damage and plastic hardening; von Mises yield criterion and isotropic hardening behavior. The total mechanical energy is written in terms of nodal positions (instead of displacements) according to Eq. 1 (Clough and Penzien 1975; Felipe and Beck 2021; Paultre 2011):

$$\Pi(\boldsymbol{z}) = U + K + Q + P = \int_{V_0} \Psi[\varepsilon(\boldsymbol{z}), D, \varpi] dV_0 + \frac{1}{2}\int_{V_0} \rho \dot{\mathbf{z}} \cdot \dot{\mathbf{z}} dV_0 + \oint \boldsymbol{F}_d(\boldsymbol{z}) d\boldsymbol{z} - \boldsymbol{F}_e \cdot \boldsymbol{z} \tag{1}$$

where U is the strain energy; K is the kinetic energy; Q is the dissipated energy; P is the potential energy of the applied forces; $\boldsymbol{z}$ is the vector of nodal positions in the current configuration; Ψ is the Helmholtz free energy potential; V_0 is the initial volume, related to the initial configuration; D is the damage variable; ϖ is the internal hardening variable; $\dot{\boldsymbol{z}}$ is the velocity vector, in the current configuration, of a general point inside the domain; ρ is the mass density related to the initial configuration; $\boldsymbol{F}_d$ is the damping force vector; and $\boldsymbol{F}_e$ is the applied external force vector. Theoretical and implementation details are given in (Felipe et al. 2019) and (Felipe and Beck 2021). This formulation does not take into account the effects of eccentric connections, initial imperfections, and instability.

3 MATERIAL FAILURE MODELLING

Figure 1a shows typical stress-strain curves for elastic, elastoplastic and hyperelastic structural materials. Typically, elastic materials have higher strength and higher Young´s modulus in comparison to elastoplastic materials; whereas

hyperelastic materials show much larger strains before failure, and much smaller Young´s modulus. We do not consider the unloading part of the elastoplastic curve as this part is not usually considered in structural design.

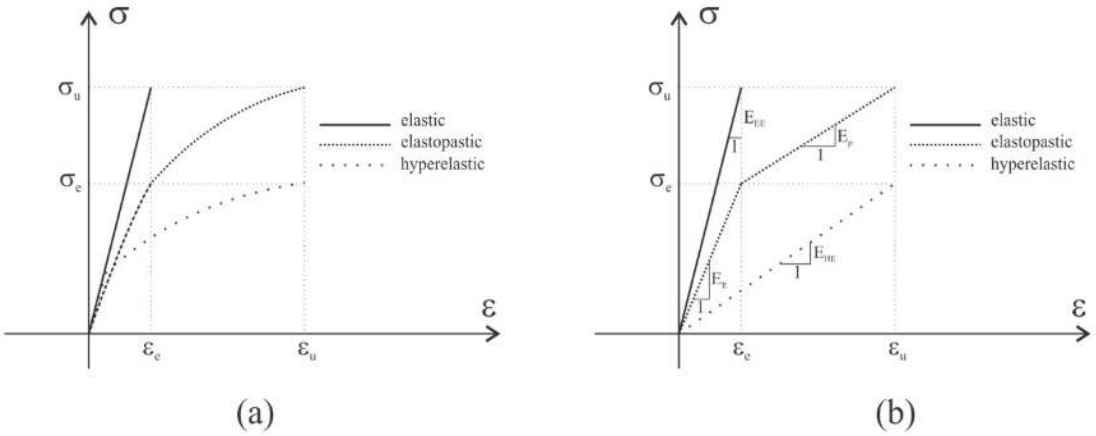

Figure 1 – ***(a)*** Typical material failure models; and (b) Linearized "equivalent" material failure models used in this paper.

Figure 1b shows simplified material models used in this paper. In order to establish some equivalence between the material failure models, we consider the same ultimate stress σ_u for the elastic and elastoplastic materials, with same elastic strain limit ε_e. Also, we consider the same ultimate strain limit ε_u for the elastoplastic and hyperelastic materials. Importantly, these models are representative of real structural materials, but the "equivalences" above do not necessarily reflect actual material triplets.

We also consider that $\sigma_u = 3\,\sigma_e/2$, and that $\varepsilon_u = 3\,\varepsilon_e$. Hence, the relationship between the Young´s modulus shown in Figure 1b are given by Equation 2.

$$E_E = \frac{\sigma_e}{\varepsilon_e}; \quad E_{EE} = \frac{\sigma_u}{\varepsilon_e} = \frac{3}{2}E_E; \quad E_P = \frac{(\sigma_u - \sigma_e)}{(\varepsilon_u - \varepsilon_e)} = \frac{1}{4}E_E; \quad E_{HE} = \frac{\sigma_e}{\varepsilon_u} = \frac{1}{3}E_E. \tag{2}$$

4 STRUCTURAL FAILURE MODELLING

Structures and structural elements are designed to accomplish some functionality. In order to accomplish this functionality, structures are required to remain in equilibrium under the action of environmental and imposed loads. This leads to the concept of service and ultimate (equilibrium) failure modes, and corresponding service and ultimate limit states. More recently, the concept of performance-based engineering has also highlighted the importance of considering intermediate failure modes like fully operational, operational, life safety and collapse prevention. The simplified material models in Figure 1b, and the simple truss structures addressed herein, are not appropriate for a characterization of performance-based design. Yet, in comparing optimal designs considering different material behavior and progressive collapse of hyperstatic structures, we try to advance towards performance-based design.

In this manuscript, we do not consider the functionality of the trusses; hence we do not address typical service failure modes. Yet, we address progressive collapse of hyperstatic elastic, elastoplastic and hyperelastic structures. A local element failure which does not lead to global collapse can be categorized as a service failure, as its consequences include loss of revenue due to downtime and cost of repair action.

For structural systems, or structures composed of multiple elements, it is important to distinguish between local failure of individual elements, progressive failure of individual elements (damage propagation), leading (or not) to partial or full collapse, and global failure modes (Tessari et al. 2019). This requires a distinction between isostatic and hyperstatic structures, between quasi-static and dynamic loading, and a connection to the type of structural failure, which in the limit can be brittle or ductile. Hyperstatic structures are characterized by the degree of static indeterminacy (DSI), which represents the difference between the number of static unknowns (reactions and internal forces) and the number of static equilibrium equations. For an isostatic structure DSI = 0, and a single element (rupture type of) failure leads to global loss of equilibrium. For an hyperstatic structure with DSI = 2, three element failures are required to produce loss of equilibrium. These rules apply to the whole structure, but also to parts of it. Progressive failure involves load redistribution within the structure. The type of loading and type of failure are strongly connected, due to the dynamic load amplification (DLA) which occurs especially under elastic fracture.

Table 1 is a tentative to summarize the relations between type of structure, type of material failure, and type of failure mode.

Table 1 – Grid of type of structural versus material failures.

	Failure mode	Brittle	Ductile
Service failure	Service failure normally occurs below or at the elastic limit; hence there are not many differences w.r.t. material failure		
Ultimate failure	Element rupture in isostatic structure (global collapse)	Instantaneous, no warning, high DLA, α_{GB}	Warning due to plastic strain, small or no DLA, α_{GD}
	Rupture of redundant member of hyperstatic structure (damage propagation)	Only relevant for large DSI and small DLA	Only "service" type of failure if progressive collapse can be avoided, α_I
	Local or global collapse due to damage propagation (progressive collapse)		Ample warning due to redundant element failures allowing preventive measures and evacuation, α_{PC}.

DSI = Degree of Static Indeterminacy; DLA = Dynamic Load Amplification; α = failure mode cost factor used in risk analysis.

Failure consequences are significantly different for the different boxes in Table 1, even if the same use and environment are considered. Brittle failures occur instantaneously, with little to no warning, not allowing for preventive measures nor evacuation, for instance. Due to lack of redundancy, brittle failure of an element of an isostatic structure, or global failure, have the largest consequences. For redundant hyperstatic structures, brittle failures will only occur in a progressive manner if DSI is large and DLA is small; otherwise, progressive failure also occurs instantaneously, due to dynamic amplification in load redistribution. This last case is not studied herein. Consequences of global brittle failures are quantified with factor α_{GB} herein, where *G* is for Global and *B* is for Brittle, as detailed later.

Ductile failure of elements of isostatic structures, or global ductile failures, have smaller consequences, since plastic strain produces reserve capacity, and serves as warning before reaching the ultimate capacity. Consequences of global ductile failures are quantified with factor $\alpha_{GD} < \alpha_{GB}$, where *D* is for Ductile.

Typically, the failure of ductile hyperstatic structures occurs in a progressive manner, following local damage to one or more elements. Such damage can lead to complete loss of strength of the affected elements, such as in brittle failure, or partial loss, as in ductile failure. Importantly, the type of material failure is relevant to the way that loads are redistributed to adjacent remaining elements, during damage propagation. As mentioned before, brittle structures with small DSI and/or large DLA may have little capacity to sustain local damage and redistribute loads, reducing the effect of redundancy. Yet, for ductile hyperstatic structures, the failure pattern will be significantly different. As damage propagation gives more warning before total collapse, we consider a consequence factor $\alpha_{PC} < \alpha_{GD} < \alpha_{GB}$, where subscript $(\cdot)_{PC}$ is for progressive collapse. If local damage is contained, the consequences are limited to loss of revenue due to downtime, and to repair of failed elements. To account for the consequences of individual element failures, we use $\alpha_I \ll \alpha_{PC} < \alpha_{GD} < \alpha_{GB}$.

The actual values of consequence multiplication factors considered in this section will vary significantly with structural use and surrounding environment. For real structures, these values should be determined based on risk analysis. In this manuscript, we focus on the relative order of magnitude of these consequence factors. In this manuscript, we consider $\alpha_I = 5 \ll \alpha_{PC} = 25 < \alpha_{GD} = 50 < \alpha_{GB} = 100$, unless otherwise stated. These are considered as multiples of the construction costs, as detailed in the sequence.

5 COST FUNCTIONS

The construction cost (CC) is written in terms of the cost of materials, given by:

$$CC(\boldsymbol{d}) = \sum_{i=1}^{n} (A_i L_i)\, \rho u \tag{3}$$

where $\boldsymbol{d}$ is the design vector, A_i is the cross-section area of bar *i*, L_i is the length of the bar *i*, ρ is the mass density and u is the unit cost of material (per weight). The reference cost for calculating the consequences of failure is the construction cost for the initial design, $C_{ref} = CC(\boldsymbol{d}_0)$.

The costs of failure are evaluated as $\alpha\, C_{ref}$, with α´s given in Section 4. The expected costs of failure, for the kth failure mode, are given as the product of the failure probability by the cost of failure:

$$ECF_k = \alpha_k \, C_{ref} \, P[g_k(\boldsymbol{d}, \boldsymbol{x}) \leq 0] \tag{4}$$

where $P[g_k(\boldsymbol{d}, \boldsymbol{x}) \leq 0]$ is the probability of failure, and $\boldsymbol{x}$ is the vector of random parameters.

The total expected cost (TEC) becomes:

$$TEC = CC(\boldsymbol{d}) + C_{ref} \begin{bmatrix} \sum_{i=1}^{n} \alpha_{IF} \, P\left[g_{IF}^{i}(\boldsymbol{d}, \boldsymbol{x}) \leq 0\right] \\ + \sum_{j=1, j\neq i}^{n} \alpha_{CF} \, P\left[g_{CF}^{j}(\boldsymbol{d}, \boldsymbol{x}) \leq 0 \middle| f^{i}\right] \\ + \sum_{k=1, k\neq i, k\neq j}^{n} \alpha_{CF} \, P\left[g_{CF}^{k}(\boldsymbol{d}, \boldsymbol{x}) \leq 0 \middle| f^{ij}\right] \\ + \cdots \\ + \alpha_G \, P[g_G(\boldsymbol{d}, \boldsymbol{x}) \leq 0] \end{bmatrix} \tag{5}$$

In Eq. (5), $(\cdot)_{IF}$ is for single initial failure of the ith bar, $(\cdot)_{CF}$ is for conditional failure of the jth bar, given failure of the ith bar; or the conditional failure of the kth bar, given failure of the bars i and j; and so on, according to the DSI of the structure. Also, $(\cdot)_G$ is for global failure modes, such as snap-through.

The consequence factors in Eq. (5) change according to failure mode and type of material. For instance, α_G is equal to α_{GB} for elastic materials, and α_{GD} for plastic materials. For isostatic structures, the second and third terms inside brackets vanish, and $\alpha_{IF} = \alpha_{GB}$ or $\alpha_{IF} = \alpha_{GD}$, as a single element failure leads to collapse. For ductile hyperstatic structures and individual failures, $\alpha_{IF} = \alpha_I$. For the conditional failures, $\alpha_{CF} = \alpha_I$, if the structure remains in equilibrium. When the last bars fail, making the structure unstable, $\alpha_{CF} = \alpha_{PC}$. The conditional limit states in Eq. (5) are formulated considering the load redistribution following individual element failures.

The proper point of compromise between safety and cost is found by solving the following risk-optimization problem (Rodrigues da Silva, Torii, and Beck 2023):

$$\boldsymbol{d}^{*} = \arg min[TEC(\boldsymbol{d}) : \boldsymbol{d} \in S] \tag{6}$$

where $S = \{\boldsymbol{d}_{min} \leq \boldsymbol{d} \leq \boldsymbol{d}_{max}\}$ are side constraints.

6 PROGRESSIVE COLLAPSE EVALUATION

Let $P[f_i]$ be the individual failure probability of the ith element, and $P[f_j|f_i]$ the conditional failure probability of the jth element, given failure of the ith element. The conditional failure probability of the kth (third) element, given failure of elements *i* and *j*, is given by $P[f_k|f_{i,j}]$. Progressive collapse of a multi-member structure can potentially start by failure of any member; the failure path initiated by failure of member *i* is denoted c_i. Each failure path must contain failure of DSI+1 elements. The alternative failure paths are assumed as mutually exclusive events, such that the probability of collapse of a sub-system formed by *n* parallel members, for a structure with DSI =2, is:

$$P[collapse] = \sum_{i=1}^{n} P[c_i] = \sum_{i=1}^{n} \sum_{j=1, j\neq i}^{n} P[f_i] \cdot P[f_j|f_i] \cdot P\left[\cup_{k=1, k\neq i, k\neq j}^{n} (f_k|f_{i,j})\right] \tag{7}$$

The number of failure paths to be analyzed can be reduced by identifying the most vulnerable elements, as argued in (Felipe and Beck 2021) and detailed later in this paper.

7 NUMERICAL RESULTS

This section presents the optimal design of the von Mises truss and a two-bay cantilever truss. Results are presented in increasing order of complexity: linear elastic analysis is shown first, then the nonlinear elastic and hyperelastic solutions are accounted for and, finally, the nonlinear plastic solution is considered. Also, the optimal design of the two-bay cantilever truss is calculated through nonlinear dynamic analysis. These solutions are compared and discussed in the following. In the mechanical analysis, a convergence tolerance of 10^{-6} is considered, based on the norm of position changes in accordance with (Felipe and Beck 2021). Probabilities of failure (P_f) are assessed through Weighted Average Simulation Method (WASM) proposed by (Rashki et al. 2012). The number of WASM samples is ns = $2 \cdot 10^6$. By way of WASM, limit state functions need to be evaluated only once, for each sample point, and before entering the optimization routine. During the optimization, only the weights of each sample need to be updated (Rashki et al. 2014). This

significantly speeds the computations. Firefly Algorithm (FA) is employed to solve the risk optimization problem (Yang 2010). The values of the parameters for FA are: $\gamma = 0.70$; $\beta_0 = 1.0$; $\alpha_0 = 0.95$; and $n_{firefly} = 10$. Table 2 describes the random variables and the assigned statistical properties. In all solutions presented herein, buckling of compressed members is disregarded.

Table 2 - Statistics for von Mises truss and two-bay cantilever truss.

Variable	Mean	cov	distribution	ref.
EE	1.00EE	0.03	Lognormal	(JCSS 2001)
σ_e	$1.05\sigma_e$	0.11	Lognormal	(Ellingwood and Galambos 1983)
F_v	$1.00F_v$	0.25	Gumbel Max	(Ellingwood and Galambos 1983)
F_h	$1.00F_h$	0.25	Gumbel Max	(Ellingwood and Galambos 1983)

7.1 von Mises truss

Figure 2 presents the geometric input data of the von Mises truss. Nominal values for the parameters are as follows: b = 100 cm; h = 10 cm; $A_1 = 2.6$ cm^2; $A_2 = 2.6$ cm^2; $\rho = 7850$ kg/m^3; EE = 20000 kN/cm^2; $\sigma_e = 25$ kN/cm^2; $F_h = 5$ kN; $F_v = 20$ kN and $\phi = 0.10$ rad. Strength material parameters (for elastic, "hyperelastic" and plastic analysis) were calculated by Equation 2.

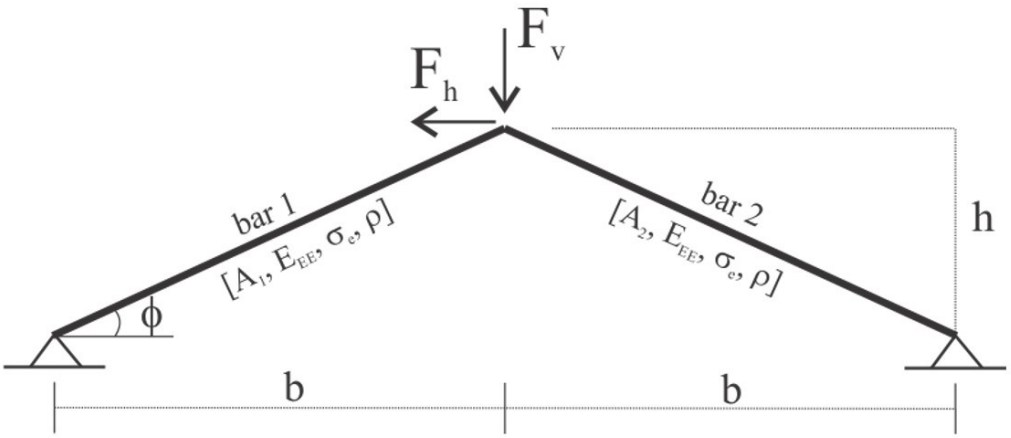

Figure 2 – Geometric input data for von Mises truss.

Vector $\boldsymbol{d}$ contains the random design variables: $\boldsymbol{d} = \{A_1, A_2\}$. The design variables are the means of normal distributed random variables with coefficient of variation (cov) equal to 0.10.

For the solution with elastic material, the limit state function for each bar is given by:

$$g_I^i(\boldsymbol{x}, \boldsymbol{d}) = \sigma_u - |\sigma_i(\boldsymbol{x}, \boldsymbol{d})| \tag{8}$$

where $(\cdot)_I^i$ indicates individual failure of the ith bar; σ_u is the ultimate stress; σ_i is the stress of bar *i*; and $|\cdot|$ is the absolute value operator.

For the solution with hyperelastic and plastic materials, the limit state function is given by:

$$g_I^i(\boldsymbol{x}, \boldsymbol{d}) = \varepsilon_u - |\varepsilon_i(\boldsymbol{x}, \boldsymbol{d})| \tag{9}$$

where ε_u is the ultimate strain; and ε_i is the strain of the bar *i*.

In the nonlinear solution when design variable h is small in comparison to b, the von Mises truss can fail due to snap-through. The limit state function for this global failure mode is

$$g_G(\boldsymbol{x}, \boldsymbol{d}) = F_{lim} - |F_v(\boldsymbol{x}, \boldsymbol{d})| \tag{10}$$

where F_{lim} is the limit force, F_v is the vertical force in node 1. The F_{lim} is the maximum force that the von Mises truss resists in a stable regime of static equilibrium before the snap-through occurrence. This force is obtained from the verification of negative eigenvalues in the Hessian matrix in a given load step of the mechanical solution.

The total expected cost (TEC) of the von Mises truss becomes:

$$TEC = \varphi_m CC(\boldsymbol{d}) + \sum_{i=1}^{n} \alpha_I \, C_{ref} \, P[g_I^i(\boldsymbol{d}, \boldsymbol{x}) \leq 0] + \alpha_G \, C_{ref} \, P[g_G(\boldsymbol{d}, \boldsymbol{x}) \leq 0] \tag{11}$$

Side constraints in Eq. (6) are $S = \{d_{min} \leq \boldsymbol{d} \leq d_{max}\} = \{2 \leq \boldsymbol{d} \leq 20\}\ [cm^2]$. Also, $\alpha_I = \alpha_G = \alpha_{GB} = 100$ because the rupture of a bar leads to direct collapse (elastic failure mode) of the von Mises truss, in accordance with Table 1. The φ_m coefficient is the relationship between the Youngs modulus of the materials, according to Table 3.

Table 4 provides a comprehensive summary of the results obtained for different solutions. Notably, as the solutions are refined, there is a consistent increase in the cross-sectional areas of the truss bars. This trend underscores the significance of iterative refinement in accurately capturing the structural response. This study emphasizes the inadequacy of the Linear Elastic (LE) solution, which fails to consider geometrical and material nonlinearities, resulting in a considerable deviation from the actual structural behavior. Furthermore, the Nonlinear Elastic (NLE) solution, while accounting for snap-through occurrences, overlooks the reduction in stiffness due to plastic strain. On the other hand, the Nonlinear Hyperelastic (NLH) solution leads to larger cross-section areas compared to the Nonlinear Plastic (NLP) solution, attributed to lower stiffness. This reduction in stiffness enhances snap-through occurrences, necessitating an increase in cross-section areas to maintain structural integrity.

Table 3 – Costs for the von Mises truss.

Solution	$\varphi_m = \frac{E_m}{E_E}$	cost of materials		total expected cost	
		mean ($)	cov (%)	mean ($)	cov (%)
LE	1.500	13.55	0.36	14.82	0.020
NLE	1.000	10.82	0.25	12.28	0.005
NLP	0.625	9.03	0.13	9.73	0.002
NLH	0.333	8.41	0.08	9.25	0.001

Note: The mean and cov are obtained from ten fireflies in one run of the algorithm.

Table 4 – Optimum solutions for the von Mises truss.

Solution	Design variables			
	A_1		A_2	
	mean (cm^2)	cov (%)	mean (cm^2)	cov (%)
LE	5.79	0.58	5.66	0.53
NLE	6.88	0.31	6.83	0.35
NLP	9.33	0.35	8.99	0.40
NLH	16.04	0.25	15.93	0.22

Note: The mean and coefficient of variation (cov) were obtained from ten fireflies in one run of the algorithm.

Figure 3 depicts the equilibrium paths of the von Mises truss under different solutions. These curves, derived from the mean values of random variables and optimal design variables (Table 4), offer valuable insights into the structural behavior. Notably, the optimal solutions converge to a linear elastic pattern, accompanied by an increase in the cross-sectional areas of the truss bars. This transition underscores the dynamic nature of the structural response and highlights the importance of adapting design parameters to achieve optimal performance. In conclusion, the comparative analysis of structural solutions for the Von Mises truss provides valuable insights into the complex interplay between material properties, geometric complexities, and structural behavior. By scrutinizing the discrepancies between linear and nonlinear solutions and delineating the implications for design, the study contributes to the advancement of structural engineering knowledge. Continued research efforts in this domain are crucial to address emerging challenges and drive innovation in structural mechanics.

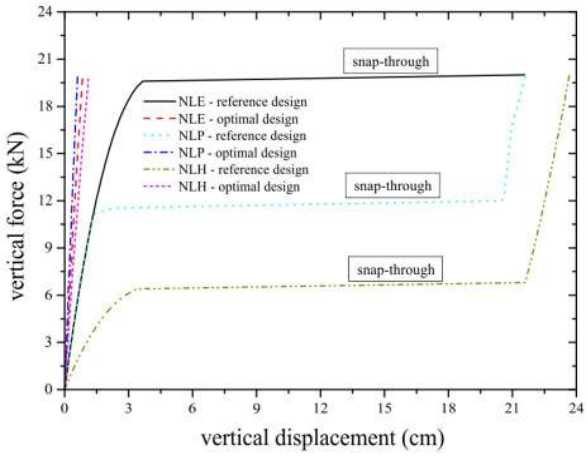

Figure 3 – Comparison of load-displacement responses, for initial (reference) designs, and for optimal solutions.

7.2 Two-bay cantilever truss

Figure 4 presents the geometric input data of the two-bay cantilever truss. The mechanical analysis of this truss was studied by (Noor and Peters 1980; Zhu et al. 1994). Here the risk-based optimization of this structure is performed. Young`s modulus, yield stress, density, and damping rate are given as EE = 200 GPa; σ_e = 250 MPa; ρ = 7850 Kg/m^3; and ξ = 0.05. Strength material parameters for plastic analysis were calculated by Equation 2. Initial cross-section area of the bars for the reference design are A1 = A2 = A3 = A4 = 200 mm^2. For dynamic analysis, the Newmark parameters are β_n = 0.25; γ_n = 0.50; and $\Delta t = 10^{-4}$ s. The amplitude of external force is $f_0 = 10^5$ N.

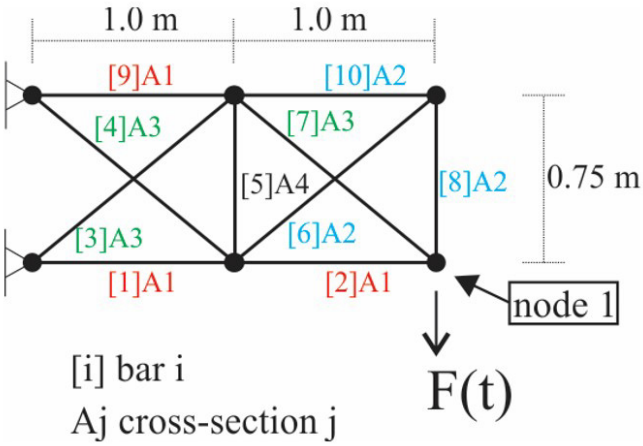

Figure 4 – Input data for two-bay cantilever truss: geometry.

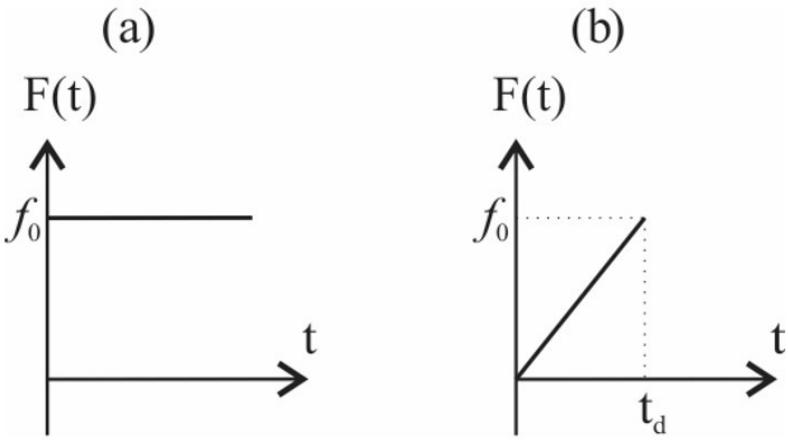

Figure 5 – Input data for two-bay cantilever truss: (a) step load; and (b) linearly increasing force.

A step load is a discontinuous force that suddenly changes from zero to a constant value f_0, as illustrated in Figure 5(a). The step load is defined as:

$$F_v(t) = \begin{cases} f_0 & \text{for } t \geq 0 \\ 0 & \text{for } t < 0 \end{cases} \tag{12}$$

A linearly increasing force is a continuous force which is increased up to a finite value f_0, corresponding to time t_d, as illustrated in Figure 5(b). The linearly increasing force can be expressed as:

$$F_v(t) = \left(\frac{f_0}{t_d}\right) t \quad \text{for } 0 \leq t \leq t_d \tag{13}$$

Figure 6 show the displacement time histories, for the step load and linearly increasing force, respectively. These responses were obtained used the reference design. Remark that step load produces greater vertical displacement than linearly increasing force. This is due to the rate of loading, as step load is suddenly applied. The rate of loading also affects the appearance of plastic strains in the bars. For the step load, plastic strains appear in all bars, except bar 5, according to Figure 7(a). On the other hand, for linearly increasing force plastic strains appear only in bars 1, 6, 7 and 9, as illustrated in Figure 7(b).

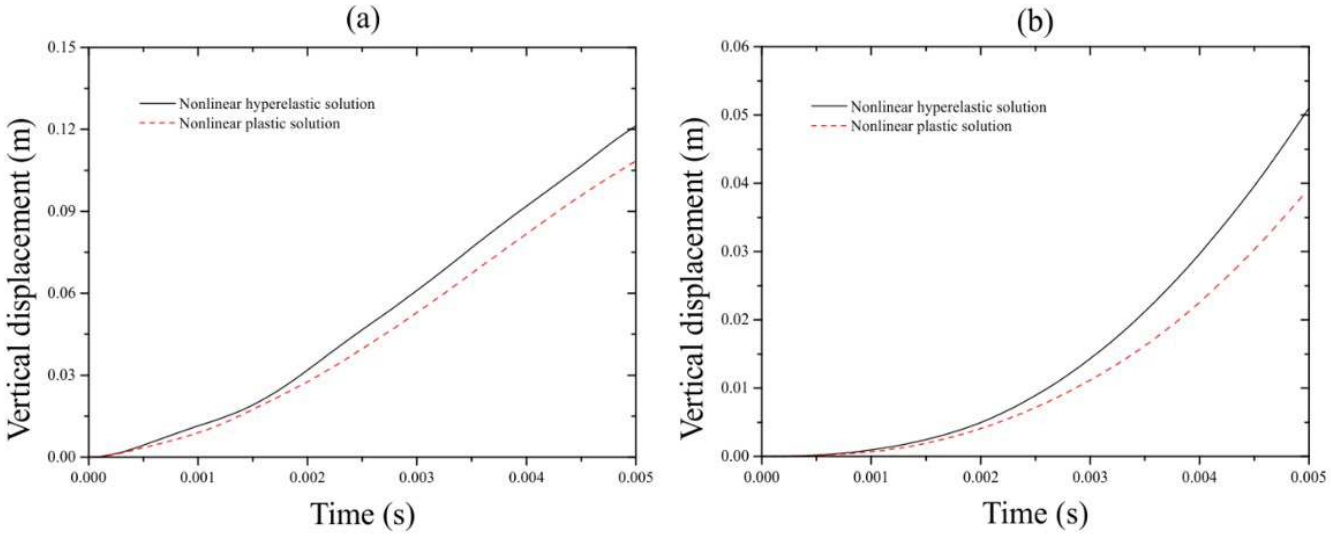

Figure 6 – Displacement time histories of the two-bay cantilever truss: (a) step load; and (b) linearly increasing force. Responses were obtained using the reference design.

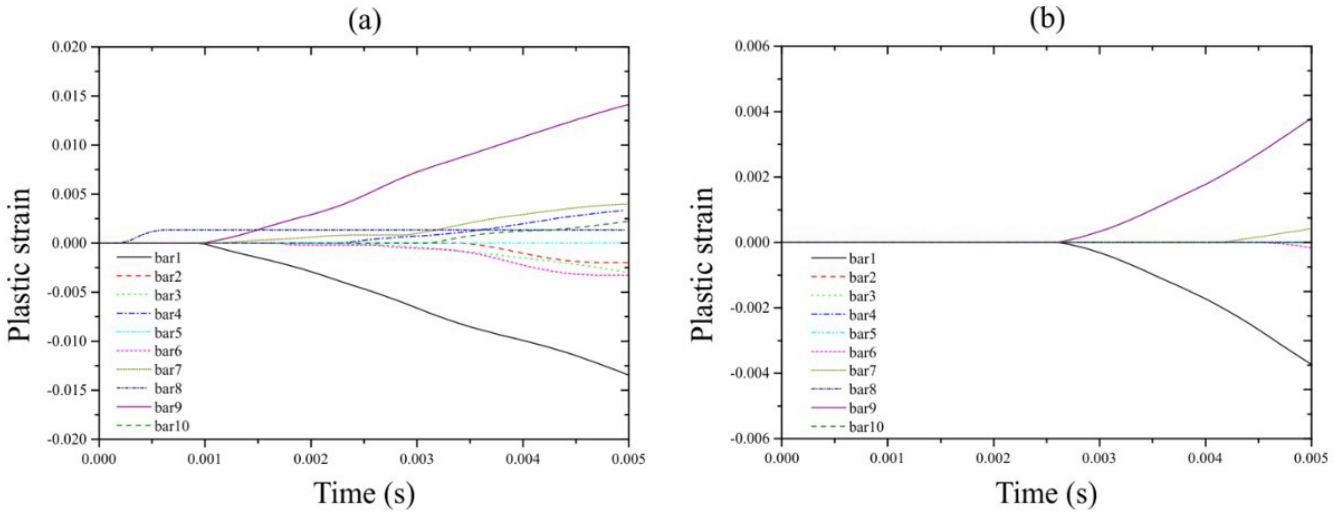

Figure 7 – Plastic strains of the two-bay cantilever truss: (a) step load; and (b) linearly increasing force. Responses were obtained using the reference design.

For the reliability analysis, the limit state function for hyperelastic and plastic materials is given by Equation (9). As the structure is hyperstatic, it is necessary to determine the most vulnerable bars to initiate the progressive collapse. For this purpose, the SRAPC (Systematic Reliability-based Approach to Progressive Collapse) methodology is used (Felipe et al. 2018). Figure 8 shows the values of the coefficient of vulnerability (CV) for each bar for different analyses. It becomes evident that the most vulnerable elements, for this hyperstatic truss, are bars number 1 and 9, followed by bars 7 and 6. The CV for bar 5 is virtually zero, showing that a primary failure of this bar would have few consequences, unlikely to lead to progressive collapse. As commented in (Felipe and Beck 2021) bars 1 and 9 fail due to the accumulation of damage because of the mechanical degradation process.

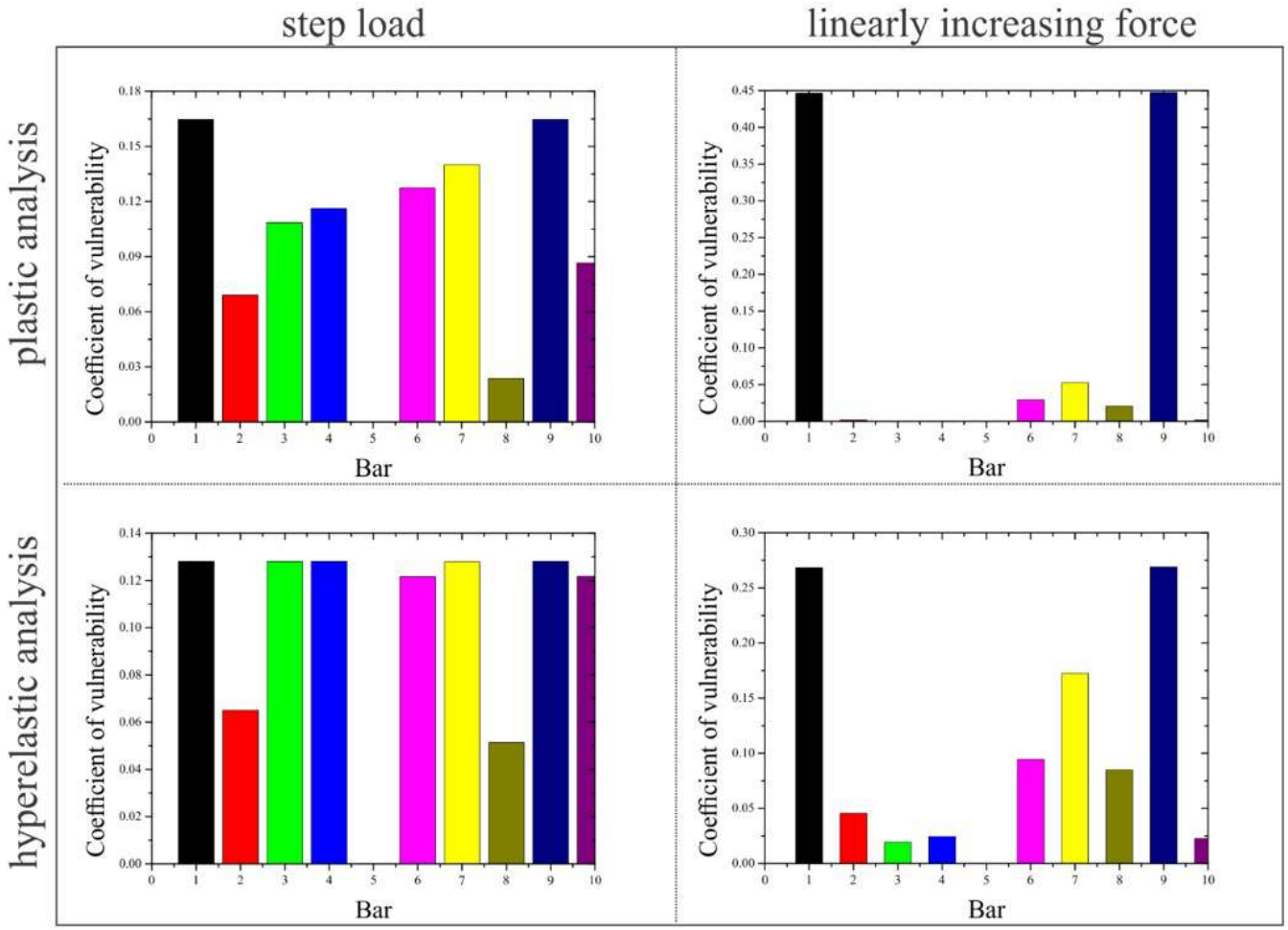

Figure 8 – CV for each bar for different analyses. Responses were obtained using the reference design.

If bars 1 and 9 fail, this leads to truss collapse due to hypostatic condition. Thus, by the SRAPC methodology, the probability of collapse ($P[collapse]$) can be evaluated by Equation (14):

$$P[collapse] \cong P[b_1] \cdot P[b_9|b_1] \tag{14}$$

where $P[b_1]$ is the probability of failure of bar 1; and $P[b_9|b_1]$ is the conditional probability of failure of bar 9, given failure of bar 1.

The total expected cost (TEC) of the two-bay cantilever truss becomes:

$$TEC = \varphi_m CC(\boldsymbol{d}) + \sum_{i=1}^{n} \alpha_I \, C_{ref} \, P[g_I^i(\boldsymbol{d}, \boldsymbol{x}) \leq 0] + \alpha_G \, C_{ref} P[collapse] \tag{15}$$

where $\boldsymbol{d} = \{A_1, A_2, A_3, A_4\}$ contains the design variables, which are the means of the corresponding random variables; and $S = \{d_{min} \leq \boldsymbol{d} \leq d_{max}\} = \{(1 \leq A_1, A_3 \leq 20), (0.1 \leq A_2, A_4 \leq 2)\}\ [cm^2]$ being side constraints. Random design

variables are represented by a normal distribution with the coefficient of variation equal to 0.10. Here, $\alpha_I = 5$ because the rupture of a hyper-static member does not lead to progressive collapse. This is considered a service failure. For the cost of collapse (ultimate failure), $\alpha_G = 25\delta$ is assumed. In the search for the optimal design of the truss, if failure of a second bar occurs, after failure of a redundant member, $\delta = 1$; but if the truss collapses directly, due to the failure of an isostatic member, $\delta = 4$.

Tables 5 and 6 present a summary of the results. Note that the nonlinear hyperelastic solution (NLH) leads to a larger cross-section area for the bars, due to the lower stiffness compared to the nonlinear plastic solution (NLP). Also, the optimal cross-section areas of the bars depend on the type of load applied. This is due to the rate of loading, as step load is suddenly applied, whereas linearly increasing force is incrementally applied. In Tables 5 to 8, the mean and coefficient of variation (cov) were obtained from ten fireflies at the endd of one run of the algorithm.

Figures 9 and 10 show the displacement time histories and the plastic strains of the optimal designs, respectively. These figures can be compared with Figures 6 and 7 for the reference truss. As noted, the optimal trusses show reduced vertical displacemens and reduced plastic strains, especially for the step load case.

Table 5 – Results for the two-bay cantilever truss: step load.

Solution	Design variables							
	A1		A2		A3		A4	
	mean (cm²)	cov (%)	mean (cm²)	cov (%)	mean (cm²)	cov (%)	mean (cm²)	cov (%)
NLP	10.00	0.95	1.89	1.55	4.58	1.37	1.00	0.86
NLH	19.00	0.54	2.00	0.00	10.80	0.58	1.56	0.50

Table 6 – Results for the two-bay cantilever truss: linearly increasing force.

Solution	Design variables							
	A1		A2		A3		A4	
	mean (cm²)	cov (%)	mean (cm²)	cov (%)	mean (cm²)	cov (%)	mean (cm²)	cov (%)
NLP	4.11	2.33	2.00	0.00	1.00	0.00	0.11	13.73
NLH	7.00	0.84	2.00	0.54	4.18	0.77	1.66	0.79

Table 7 – Costs for the von Mises truss: step load.

Solution	$\varphi_m = \frac{E_m}{E_E}$	cost of materials		total expected cost	
		mean ($)	cov (%)	mean ($)	cov (%)
NLP	0.625	26.27	0.88	32.13	0.11
NLH	0.333	27.39	0.34	32.39	0.01

Table 8 – Costs for the von Mises truss: linearly increasing force.

Solution	$\varphi_m = \frac{E_m}{E_E}$	cost of materials		total expected cost	
		mean ($)	cov (%)	mean ($)	cov (%)
NLP	0.625	10.87	1.30	11.34	0.32
NLH	0.333	14.41	0.17	11.49	0.51

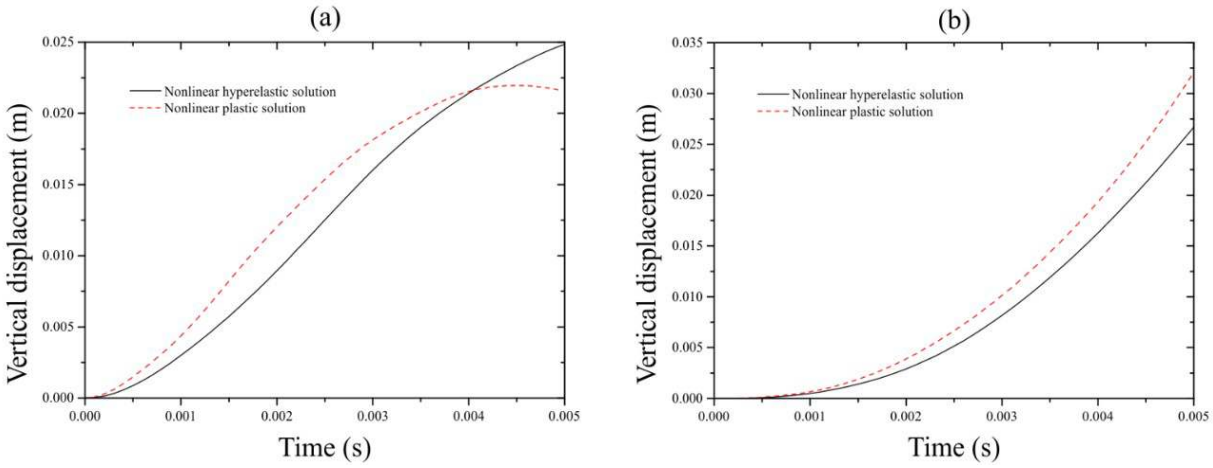

Figure 9 – Displacement time histories of the two-bay cantilever truss: (a) step load; and (b) linearly increasing force. Responses were obtained using the optimal designs.

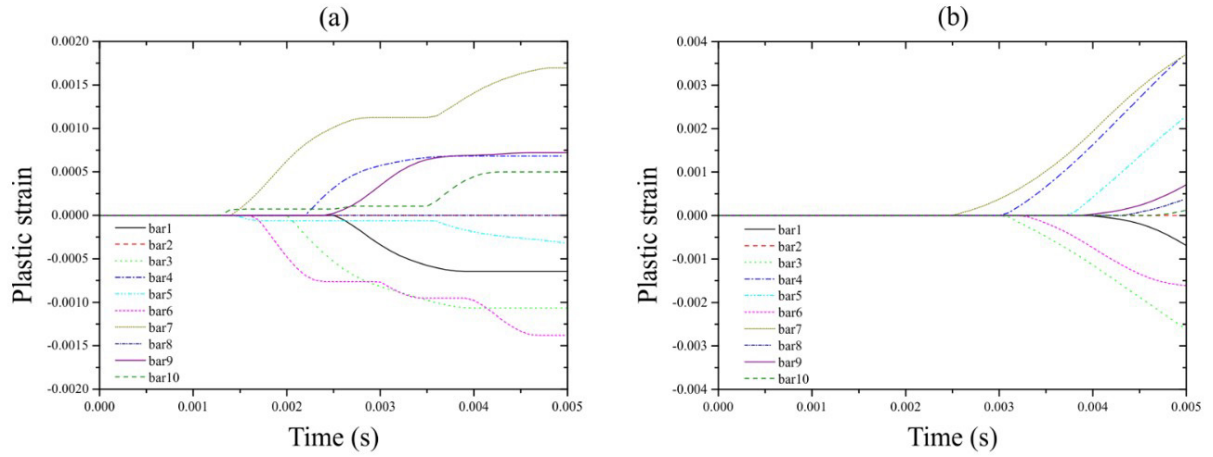

Figure 10 – Plastic strains of the two-bay cantilever truss: (a) step load; and (b) linearly increasing force. *Responses were obtained using the optimal designs.*

Figure 11 shows the coefficients of vulnerability for the different bars of the optimal trusses. The comparison between Figure 11, Figure 8, and the results presented in Tables 5 and 6 reveals insightful patterns regarding the impact of structural modifications on the vulnerability of truss elements. Specifically, the increase in the cross-sectional area (A1) of bars 1 and 9 appears to have effectively reduced the vulnerability of these bars to failure. This observation aligns with the expected outcome, as reinforcing critical elements can enhance the overall stability of the structure.

However, the analysis also highlights a nuanced effect on the vulnerability of other bars, notably bar 7. Despite the increase in cross-sectional area (A3) for most optimum truss designs, the vulnerability of bar 7 seems to have heightened. This intriguing finding underscores the complexity inherent in structural modifications and their implications for vulnerability mitigation. It suggests that while reinforcing certain elements may bolster structural integrity, it can inadvertently redistribute stress and increase vulnerability in other areas.

This intricate interplay between structural modifications and vulnerability mitigation strategies underscores the importance of comprehensive design considerations. Engineers must carefully assess not only the direct impact of modifications but also their potential ripple effects on the overall structural behavior. By leveraging insights from displacement responses and reliability assessments, engineers can effectively navigate these complexities and devise robust mitigation strategies.

In essence, the analysis presented in the text underscores the paramount importance of holistic approaches to structural design and evaluation. By integrating insights from displacement responses and reliability assessments, engineers can iteratively refine designs to enhance resilience and safety against diverse loading scenarios. This proactive approach enables the creation of structures that not only withstand anticipated loads but also exhibit robustness in the face of unforeseen challenges.

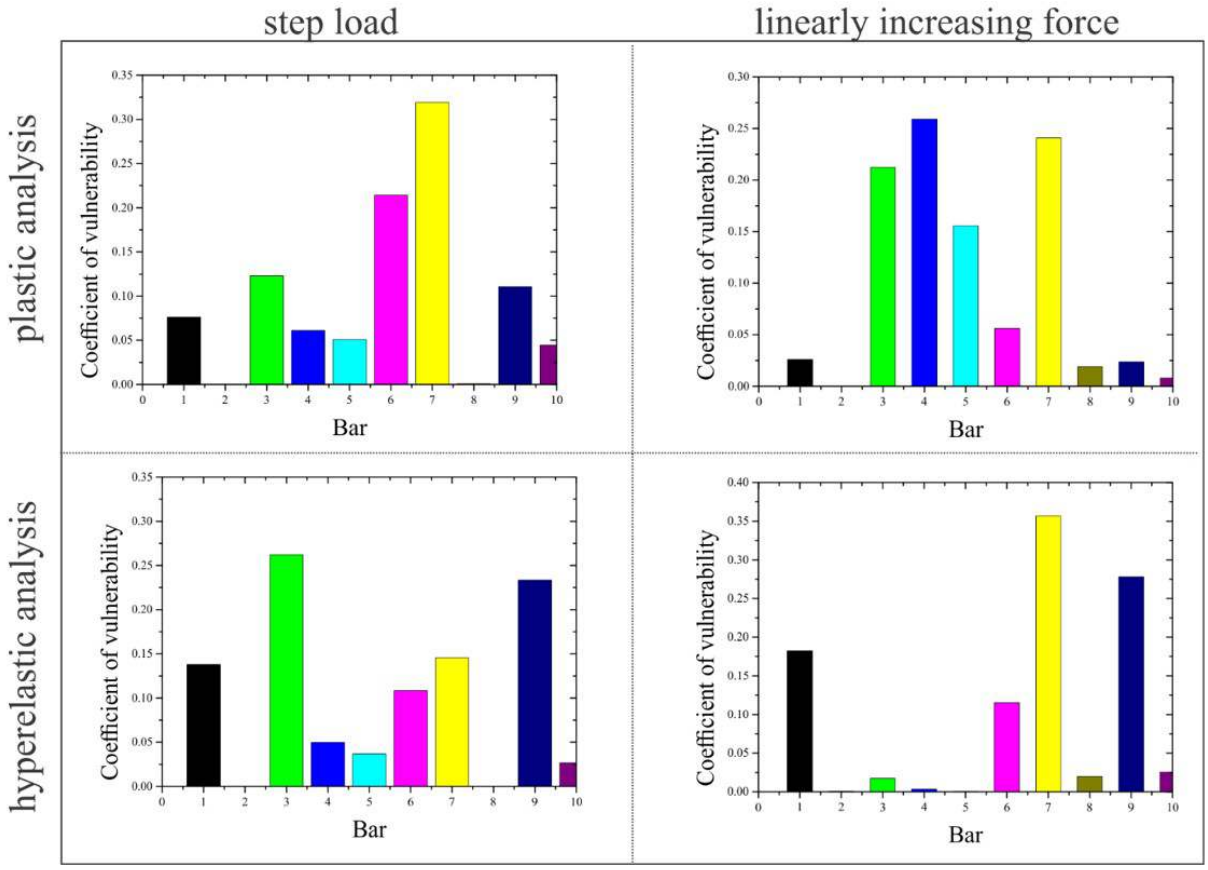

Figure 11 – CV for each bar for different analyses. Responses were obtained using the optimal designs.

The formulation proposed herein for the optimal design of nonlinear truss structures considering progressive collapse leads to simple mathematical formalism, easy numerical implementation, and low computational cost. This last claim is evaluated by an analysis of computer processing times, as reported in Table 9. Numerical solutions were computed on an Intel Core i7-8550U processor, with clock speed of 1.80 GHz. Analyses were obtained with $n_S = 2 \cdot 10^6$ samples of Weighted Average Simulation Method, and $n = 10^2$ load steps. Consequently, for each load case (step load and linearly increasing force), the numerical model was evaluated $2 \cdot 10^8$ times. As observed in Table 9, the risk optimization considering nonlinear dynamic solutions reported in this paper were obtained within very small computation times.

Table 9 – Processing time of the analyses.

Type of Loading	Analysis	Processing time (s)
Response to a step load	Plastic	$8.4710 \cdot 10^3$
	Hyperelastic	$4.4227 \cdot 10^3$
Response to linearly increasing force	Plastic	$6.5434 \cdot 10^3$
	Hyperelastic	$6.3440 \cdot 10^3$

8 CONCLUSION

This paper introduces a comprehensive methodology aimed at evaluating the optimal design of truss structures subjected to progressive collapse. The proposed approach integrates various analytical techniques, including total-Lagrangian formulation for material and geometrical nonlinear analysis, systematic reliability-based approach to progressive collapse, and risk-based optimization. Additionally, the study utilizes the ductile-damage FLHB model for nonlinear static and dynamic analysis.

Through the examination of two academic benchmark examples, the effectiveness and stability of the proposed methodology are demonstrated. The results indicate that the methodology efficiently evaluates optimal truss designs under progressive collapse scenarios. Furthermore, it is revealed that material behavior (elastic, elastoplastic, and hyperelastic) and the rate of loading (step and linear load) significantly influence the configurations of optimal truss designs.

Specifically, the optimal solution for the von Mises truss is characterized by a linear elastic response with an increasing cross-section of bars. Moreover, the convergence of optimal design for the two-bay cantilever truss, a hyper-static structure, is shown to depend on the coefficient of vulnerability. Notably, the optimization process leads to a reduction in the vulnerability of the most critical bars in the reference design, resulting in load redistribution and the establishment of alternate load paths. This redistribution effectively mitigates the probability of progressive collapse occurrence.

In conclusion, the study underscores the importance of adopting a holistic approach to truss structure optimization. By integrating considerations of uncertainties, progressive collapse, and advanced analysis techniques, engineers can develop resilient and efficient truss structures capable of withstanding extreme loading conditions while minimizing the risk of catastrophic failure. This holistic approach not only enhances structural safety but also contributes to the advancement of structural engineering practices in mitigating the effects of unexpected events.

ACKNOWLEDGEMENTS

The authors acknowledge funding of this research project by Brazilian agencies CAPES (Brazilian Higher Education Council – Finance Code 001), CNPq (Brazilian National Council for Research) and FAPESP (São Paulo State Research Foundation, grant n. 2019/13080-9).

Author's Contribuitions: TRCF: resources, computer programming, writing original draft; ATB: conceptualization, funding acquisition, methodology, supervision, writing original draft, writing-review editing.

Editor: Marco L. Bittencourt

References

Ayyub, B. M. and G. J. Klir. 2006. *Uncertainty Modeling and Analysis in Engineering and the Sciences.* Boca Raton, FL: Chapman & Hall/CRC.

Beck AT, 2020: Optimal Design of Hyperstatic Redundant Structural Systems: fundamentals, Engineering Structures 219, 110542. https://doi.org/10.1016/j.engstruct.2020.110542

Beck AT, Rodrigues da Silva LA, and Miguel LFF, 2023: The Latent Failure Probability: a conceptual basis for Robust, Reliability-based and Risk-based Design Optimization, Reliability Engineering & System Safety 233, 109127, https://doi.org/10.1016/j.ress.2023.109127

Clough, R. W. and J. Penzien. 1975. *Dynamics of Structures.* Tokyo: McGraw-Hill.

Ellingwood, Bruce and Galambos, T.V.. 1983. "Probability-Based Criteria for Structural Design." *Structural Safety* 1(1):15–26.

Felipe, T. R. C., V. G. Haach, and A. T. Beck. 2018. "Systematic Reliability-Based Approach to Progressive Collapse." *ASCE-ASME Journal of Risk and Uncertainty in Engineering Systems, Part A: Civil Engineering* 4(4).

Felipe TRC, Leonel ED, Haach VG, Beck AT, 2019: A Comprehensive Ductile Damage Model for 3D Truss Structures, International Journal of Non-Linear Mechanics 112, 13-24. https://doi.org/10.1016/j.ijnonlinmec.2019.02.010

Felipe TRC, Beck AT, 2021: Dynamic analysis of failure paths of truss structures: benchmark examples including material degradation, Mechanical Systems and Signal Processing 158, 107767. https://doi.org/10.1016/j.ymssp.2021.107767

Gomes, W. J. and A. T. Beck. 2014. "Optimal Inspection Planning and Repair under Random Crack Propagation." *Engineering Structures* 69:285–96.

JCSS. 2001. "Probabilistic Model Code - Part 1." *Structural Safety* (March):65.

Liu, Y., H. K. Jeong, and M. Collette. 2016. "Efficient Optimization of Reliability-Constrained Structural Design Problems Including Interval Uncertainty." *Computers & Structures* 177:1–11.

Melchers, R. E. and A. T. Beck. 2018. *Structural Reliability Analysis and Prediction.* New Jersey: John Wiley & Sons.

Noor, A. K. and J. M. Peters. 1980. "Nonlinear Dynamic Analysis of Space Trusses." *Computer Methods in Applied Mechanics and Engineering* 21:131–51.

Paultre, P. 2011. *Dynamics of Structures.* London: ISTE and Wiley.

Rashki, M., M. Miri, and M. A. Moghaddam. 2012. “A New Efficient Simulation Method to Aproxime the Probability of Failure and Most Probable Point.” *Structural Safety* 39:22–29.

Rashki, Mohsen, Mahmoud Miri, and Mehdi Azhdary Moghaddam. 2014. “A Simulation-Based Method for Reliability Based Design Optimization Problems with Highly Nonlinear Constraints.” *Automation in Construction* 47:24–36.

Rodrigues da Silva, L. A., A. J. Torii, and A. T. Beck. 2023. “Hyperstatic and Redundancy Thresholds in Truss Topology Optimization Considering Progressive Collapse Due to Aleatory and Epistemic Uncertainties.” *Probabilistic Engineering Mechanics* 71:103384.

Rodrigues da Silva L.A., Torii AJ, Beck AT, 2024: System-reliability-based sizing and shape optimization of trusses considering millions of failure sequences, Structural Safety 108, 102448, https://doi.org/10.1016/j.strusafe.2024.102448

Saad, L., A. Chateauneuf, and W. Raphael. 2018. “Robust Formulation for Reliability-Based Design Optimization of Structures.” *Structural and Multidisciplinary Optimization* 57(6):2233–48.

Tessari, R. K., H. M. Kroetz, and A. T. BECK. 2019. “System Reliability-Based Design Optimization and Risk-Based Optimization: A Benchmark Example Considering Progressive Collapse.” *Engineering Optimization* 51:1000–1012.

Yang, Xin-she. 2010. *Nature-Inspired Metaheuristic Algorithms*. 2nd ed. Frome: Luniver Press.

Zaman, K. and S. Mahadevan. 2017. “Reliability-Based Design Optimization of Multidisciplinary System under Aleatory and Epistemic Uncertainty.” *Structural and Multidisciplinary Optimization* 55(2):681–99.

Zhu, K., F. G. A. Al-Bermani, and S. Kitipornchai. 1994. “Nonlinear Dynamic Analysis of Lattice Structures.” *Computers & Structures* 52(1):9–15.